Contributed Paper

Observation of Resistive Wall Modes in JT-60U

TAKEJI Satoru, TOKUDA Shinji, KURITA Genichi, SUZUKI Takahiro, ISAYAMA Akihiko, TAKECHI Manabu, OYAMA Naoyuki, FUJITA Takaaki, IDE Shunsuke, ISHIDA Shinichi, KAMADA Yutaka, OIKAWA Toshihiro, SAKAMOTO Yoshiteru, TUDA Takashi and the JT-60 Team

Naka Fusion Research Establishment, Japan Atomic Energy Research Institute, Ibaraki 311-0193, Japan

(Received 5 December 2001 / Accepted 27 March 2002)

Abstract

Resistive wall modes (RWM) associated with ideal magnetohydrodynamic current-driven ($\beta_N < 0.2$) and pressure-driven ($\beta_N > 2.4$) kink modes with low toroidal mode number n ($n = 1$) have been identified in JT-60U. The pressure-driven RWM occurs at the plasma toroidal rotation of about 1% the Alfvén speed without clear continuous slowing down of the plasma toroidal rotation. Occurrence of $n = 1$ RWMs result in thermal quench accompanied by higher n ($n \geq 2$) modes. In the case of current-driven (~ zero β) RWMs, a thermal quench occurs only at the peripheral region just after the RWM. In contrast, a thermal quench occurs in the whole plasma region following a drastic increase in the growth rate of the RWM from the order of τ_w^{-1} (τ_w is the resistive diffusion time of the wall) to larger than $10^2\ \tau_w^{-1}$ in the case of pressure-driven (high β) RWMs.

Keywords:

resistive wall mode, ideal magnetohydrodynamics, low n kink, current-driven kink, pressure-driven kink, reversed shear, thermal quench, tokamak, JT-60U

1. Introduction

High β operation with a reversed magnetic shear configuration is an essential concept for an economical steady state tokamak fusion reactor. The higher β results in the larger bootstrap current and the higher fusion power at the fixed magnetic field. A reversed magnetic shear configuration is consistent with a steady state of a tokamak discharge with large bootstrap current fraction [1-3]. Magnetohydrodynamic (MHD) instabilities which limit attainable β of reversed shear discharges have been reported to be ideal kink modes with low toroidal mode numbers n in several tokamaks including JT-60U [4-7].

The stability limit of ideal low n kink modes is significantly improved by placing a perfectly conducting wall near the plasma surface. Resistive wall modes (RWMs) which are a branch of ideal low n kink modes are, however, destabilized owing to the finite resistivity of the nearby conducting wall when the ideal low n kink modes are stable with the perfect wall but unstable without the wall [8]. Since the stability limit of a reversed magnetic shear configuration against ideal low n kink modes is relatively lower than conventional configurations without a conducting wall [9], wall stabilization of ideal low n kink modes and suppression of RWMs are crucial for achievement of steady state high β reversed shear discharges.

Theoretical studies of stabilizing effects of a resistive wall have revealed that plasma rotation is essentially important for wall stabilization and suppression of RWMs [8,10-13]. Experimental studies of

author's e-mail: satoru_tak02@yahoo.co.jp

この論文は第18回年会(2001, 福岡)にて招待講演として発表された内容を論文化したものです。

stabilization of ideal low n kink modes by a nearby conducting wall have been carried out in several tokamaks [14-17]. High β_N (= $\beta/(I_p/aB_T)$ (%m·T/MA), here I_p is plasma current in MA, a is plasma minor radius and B_T is toroidal magnetic field) discharges exceeding the ideal stability limit without the wall $\beta_N^{\text{no-wall}}$ have been demonstrated for a few 10 times the resistive diffusion time of the wall τ_w with certain plasma rotation and RWM have been observed to degrade the β_N in DIII-D [14,15] and PBX-M [16]. Wall stabilization of current-driven low n external kink modes has been studied in HBT-EP [17]. Dependence of RWMs on wall coupling has been investigated by changing the plasma shape or the wall position [16,17]. Active stabilization of RWMs has been carried out by means of feedback control of the perturbed magnetic field [18,19].

In JT-60U, we have reported with respect to reversed shear discharges that the upper boundary of the achieved β_N is consistent with the theoretical $\beta_N^{\text{no-wall}}$ and resistive modes relate to major collapse in the regime $\beta_N < \beta_N^{\text{no-wall}}$ [7,20]. High β_N exceeding $\beta_N^{\text{no-wall}}$ were obtained transiently with the help of a nearby conducting wall and MHD perturbations which are attributed to the RWM was observed to terminate the high β_N discharges [20]. In this paper, direct observation of RWMs associated with both current-driven (~ zero β) and pressure-driven (high β) low n kink modes is reported from a large tokamak JT-60U. We also pay attention to the process of major collapse, which results from the growth of RWMs, in comparison between the cases of the RWMs associated with current-driven (~ zero β) and pressure-driven (high β) kink modes. Identification of the RWMs associated with current-driven and pressure-driven ideal n = 1 kink modes are described in Sec. **2** and **3**, respectively. Thermal quench following the RWMs is discussed in comparison between ~ zero β and high β cases in Sec. **4**. Results obtained in this experimental study are summarized in Sec. **5**.

2. RWMs Associated with Current-Driven Kink Modes

Current-driven ideal low n kink modes can be unstable nearly at zero β with an amount of plasma surface current with low internal inductance ℓ_i. Such situation was realized in ohmic discharges with fast plasma current ramp-up ($\dot{I}_p > 0$) and RWMs associated with a current-driven n = 1 kink mode were directly observed.

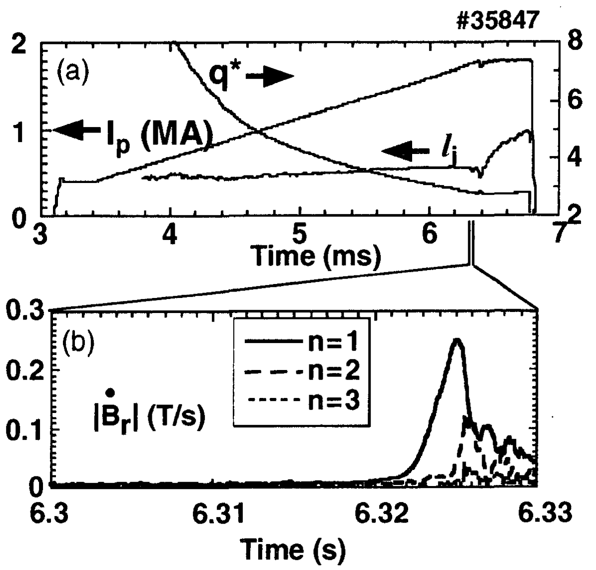

Fig. 1 Waveforms of a typical current ramp-up experiment for observation of current-driven external kink modes; (a) plasma current I_p, plasma internal inductance ℓ_i and safety factor q^*, and (b) n = 1, 2 and 3 components of time-derivative of the perturbed magnetic field in the radial direction at the occurrence of the instability.

Figure 1 shows typical waveforms of an ohmic discharge in the experiments of current-driven kink modes. Safety factor near the edge q^* decreases with increase in the plasma current and an n = 1 mode grows at $t \approx 6.319$ s just after q^* passes through three. Here, q^* is defined as $5a^2B_T/(2RI_p)[1 + \kappa^2(1 + 2\delta^2 - 1.2\delta^3)]$; R: major radius, κ: elongation, δ: triangularity. The typical plasma current ramp-up rate was 0.5 MA/s and $\ell_i \approx 0.5$. The plasma current ramp-up rate was increased up to 1.2 MA/s occasionally to destabilize the n = 1 modes at 2.5 < q^* < 3. A growth rate γ of the n = 1 mode is about 430 s^{-1} in the early phase and is about 1,020 s^{-1} at $t \approx$ 6.322 s. Since the estimated τ_w of the JT-60U vacuum vessel is ≈ 10 ms, the growth rate of 430 s^{-1} corresponds to ≈ 4 τ_w^{-1}. Toroidal rotation velocity of the ohmic discharges is nearly zero within the uncertainty of the measurement by a charge-exchange recombination spectroscopy (CXRS) [21]. The diamagnetic drift is a dominant fluid drift in the poloidal direction in such ohmic discharges and its velocity is typically ≈ 5 km/s.

Time evolution of electron temperatures T_e measured by electron cyclotron emission (ECE) heterodyne radiometers [22] at the occurrence of an n = 1 mode and the following thermal quench is shown in Fig. 2 together with perturbed magnetic field measured by eight saddle sensors located toroidally on the

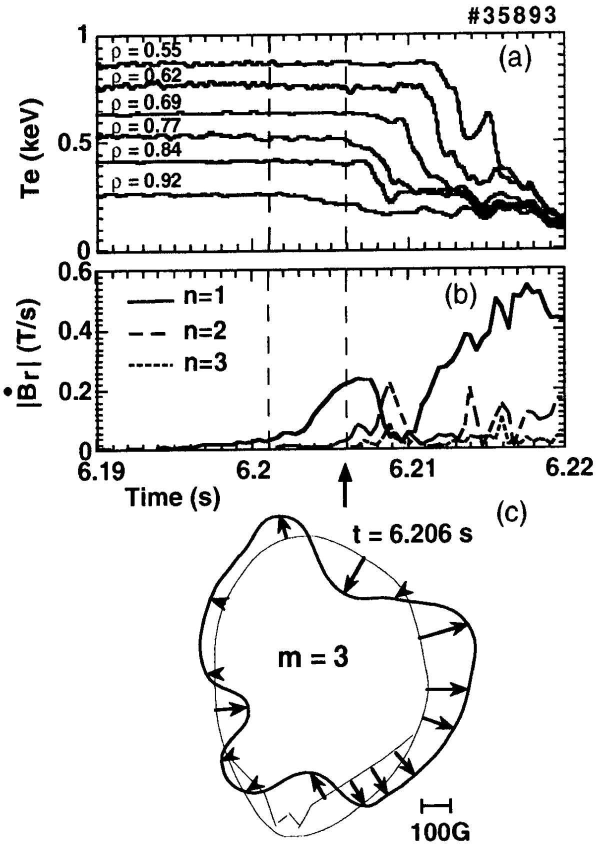

Fig. 2 Time evolution of (a) electron temperatures T_e and (b) n = 1, 2 and 3 components of time derivative of the perturbed magnetic field in the radial direction at the occurrence of the instability. The broken lines indicate the period for calculation of δT_e in Fig. 3(a). (c) Poloidal mode structure of the perturbed magnetic field showing that m = 3 is dominant.

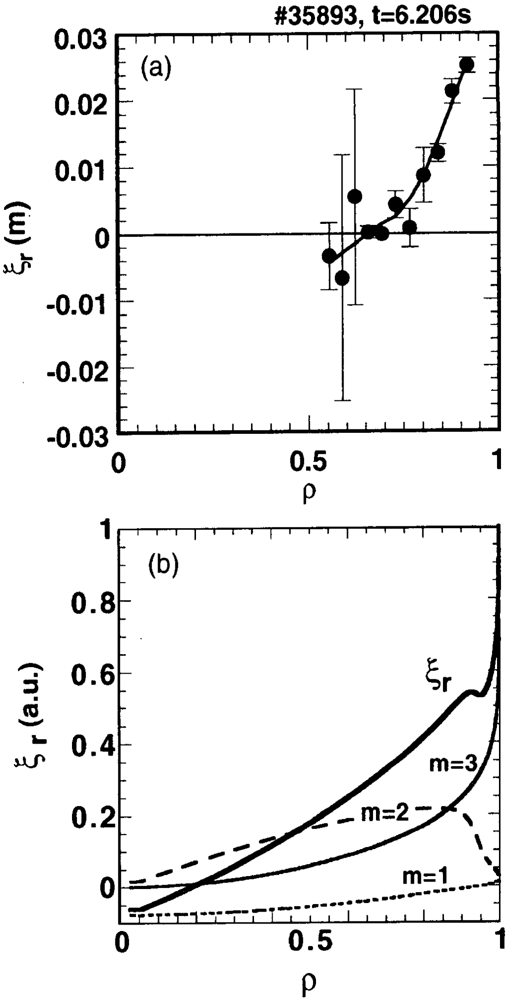

Fig. 3 Radial profiles of (a) plasma displacement in the radial direction due to the n = 1 instability estimated from T_e perturbations as $\xi_r = \delta T_e/\nabla T_e$, and (b) theoretical radial plasma displacement of a current-driven (~ zero β) n = 1 external kink mode and its Fourier components computed by the ERATO-J code.

horizontal mid-plane in the weak field side inside the vacuum vessel. A poloidal mode structure of the perturbed magnetic field mode measured by fifteen pick-up coils located poloidally on a poloidal cross-section is shown in Fig. 2(c). A radial distribution of plasma radial displacement ξ_r due to the n = 1 mode was estimated from the T_e evolution as $\xi_r = \delta T_e/\nabla T_e$ (Fig. 3(a)). Here δT_e is the change of T_e during the growth of the n = 1 mode from t = 6.201 s until t = 6.206 s in Fig. 2(a), and ∇T_e is the local gradient in the T_e profile. Figure 3(b) shows a radial profile of theoretical plasma radial displacement and its poloidal Fourier components of an ideal n = 1 external kink mode which can be unstable with a certain plasma surface current computed by the ERATO-J code [23]. The experimental profile of ξ_r clearly shows that the n = 1 mode is a global external mode and is similar to the theoretical one of an ideal n = 1 external kink mode. The fact that m = 3 is the dominant poloidal mode number of the n = 1 magnetic perturbations (Fig. 2(c)) is in agreement with that the observed mode is an ideal n = 1 external kink mode destabilized at $q^* \lesssim 3.0$. No evidence of magnetic islands nor localized MHD perturbations which is a typical characteristic of resistive MHD instabilities are observed.

The growth rate of n = 1 modes are shown as a function of the ratio of the wall radius d to the plasma minor radius a in Fig. 4. The growth rate ranges 413–1,085 s^{-1}. We confirmed from stability analysis using the ERATO-J code that an ideal n = 1 mode is stable if a perfectly conducting wall is placed at $d/a \leq 1.3$.

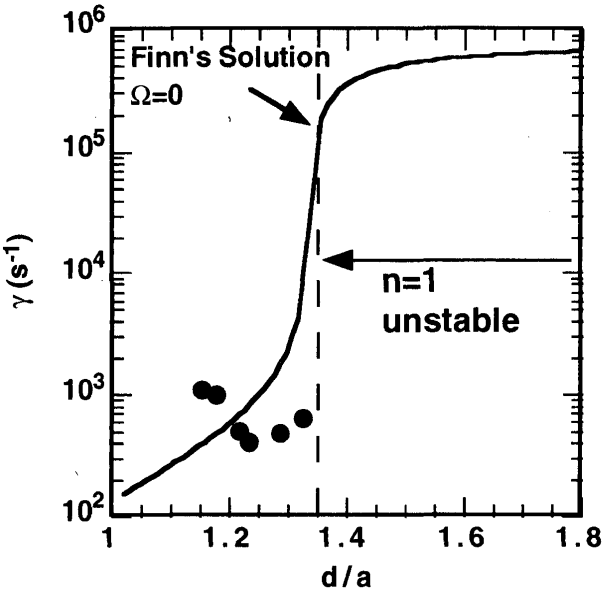

Fig. 4 Growth rate of the n = 1 external kink modes (closed circles) versus the ratio of the wall radius to the plasma minor radius d/a. Solid line is a Finn's analytical solution with the actual parameters such that B_T = 2 T, a = 1 m and $\tau_w \approx 10^{-2}$ s. The safety factor at the magnetic axis and the plasma flow are assumed to be q_0 = 2.15 and Ω = 0, respectively. Unstable region of the n = 1 mode computed by the ERATO-J code is also illustrated.

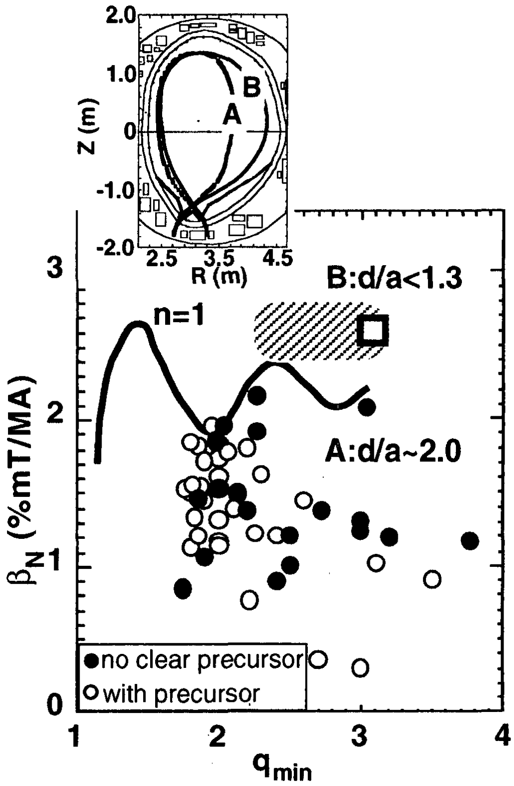

Fig. 5 Region of achieved β_N just before major collapse in reversed shear discharges with $d/a \approx 2.0$ (plasma shape A). Close circles refer to the data with no clear precursor and open circles refer to the data with clear precursor with γ > 0.3 ms. The solid line indicates the computed stability boundary of the n = 1 ideal kink-ballooning mode with the wall at infinity. An open square shows a data with $d/a \lesssim 1.3$ (plasma shape B) and the scratched region indicates an estimated region of attained β_N in the discharges with d/a < 1.3.

Theoretical growth rate of the n = 1 mode calculated from the Finn's formulation [12] with parameters similar to the experimental condition is also illustrated as a solid line. The observed growth rates are of the same order with the growth rate expected from the Finn's solution although the dependence of the growth rate on d/a is not clear.

Then, it is confirmed that the n = 1 modes which have a similar mode structure with the ideal n = 1 external kink mode are observed in the stable region with a perfectly conducting wall, and have the growth rate similar to the theoretical one with the resistive wall. Thus, we identified that the n = 1 mode is the RWM associated with the current-driven (~ zero β) ideal n = 1 external kink mode. Effects of the diamagnetic drift on the growth rate of the RWMs is not clear in this experiment.

3. RWMs Associated with Pressure-Driven Kink Modes

High β_N discharges exceeding $\beta_N^{\text{no-wall}}$ of pressure-driven ideal low n kink modes were obtained in reversed shear discharges without a plasma current ramp ($\dot{I}_p = 0$) with the help of stabilizing effect of the wall, and RWMs associated with pressure-driven ideal n = 1 kink modes were directly observed.

Figure 5 shows the region of achieved β_N just before disruptions or major collapses in reversed shear discharges. Upper limit of the achieved β_N in discharges with the wall at $d/a \approx 2.0$ is in agreement with the theoretical $\beta_N^{\text{no-wall}}$ which is calculated by the ERATO-J code with a typical experimental equilibrium [7]. Here d is the distance between the magnetic axis and the wall in the weak field side in the case of high β discharges. High β_N exceeding $\beta_N^{\text{no-wall}}$ were obtained transiently in discharges with $d/a \leq 1.3$ and n = 1 modes emerged to terminate the discharges.

Figure 6 shows radial profiles of measured plasma temperature, density and a poloidal cross section of the flux surface of a typical high β reversed shear discharge.

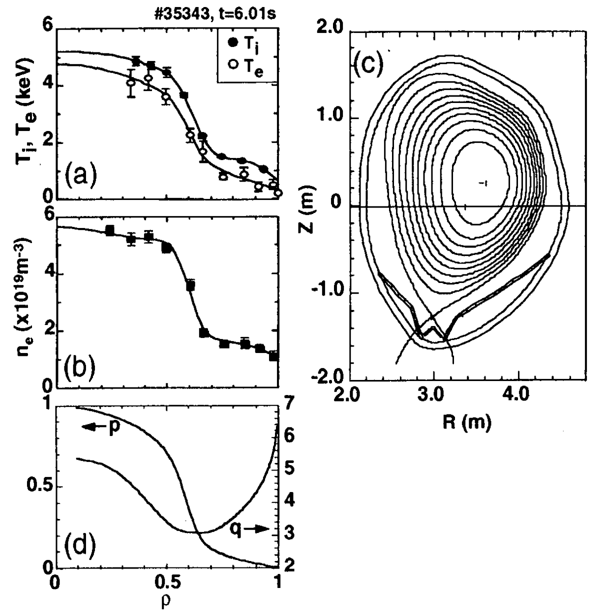

Fig. 6 Radial profiles of (a) ion temperature T_i and electron temperature T_e, (b) electron density n_e, and (c) a poloidal cross section of the flux surface of a typical high β reversed shear discharge, and (d) radial profiles of the reconstructed pressure p and the safety factor q for stability analysis.

Radial profiles of reconstructed pressure p, safety factor q are indicated in Fig. 6(d). The plasma parameters are that $I_p = 0.9$ MA, $B_T = 2.4$ T, $\ell_i \approx 0.7$, $q^* = 5.4$, $\kappa \approx 1.5$, $\delta \approx 0.38$ and $d/a \approx 1.2$. The reconstruction of an experimental equilibrium for stability analysis incorporates with measured profiles of ion temperature from the CXRS [21], electron temperature from Thomson scattering [24,25] and ECE [22], electron density from Thomson scattering and FIR and CO_2 interferometer chords [26,27], and q from motional Stark effect measurements [28]. Fast ion pressure calculated by the OFMC code [29] is also included in the pressure profile.

Figure 7 shows time evolution of plasma parameters and MHD perturbations of a reversed shear discharge in which the achieved β_N exceeded the calculated $\beta_N^{\text{no-wall}}$. The calculated $\beta_N^{\text{no-wall}}$ is ≈ 2.2 in the similar discharge with $\ell_i \approx 0.7$. The normalized β increases gradually in time and exceeds $\beta_N^{\text{no-wall}}$ at $t \approx 6$ s. The discharge is terminated in disruption at $\beta_N = 2.6$ (Fig. 7(a)). Plasma rotation frequency in the toroidal direction f_{tor} is about 4 kHz in the counter-direction to the plasma current at the radial region corresponding to the $q = 4$ surfaces. The toroidal rotation in the counter-direction to the plasma current is due to an inward electric field induced by a ripple loss of fast ions from the near-perpendicular neutral beams [30]. The time

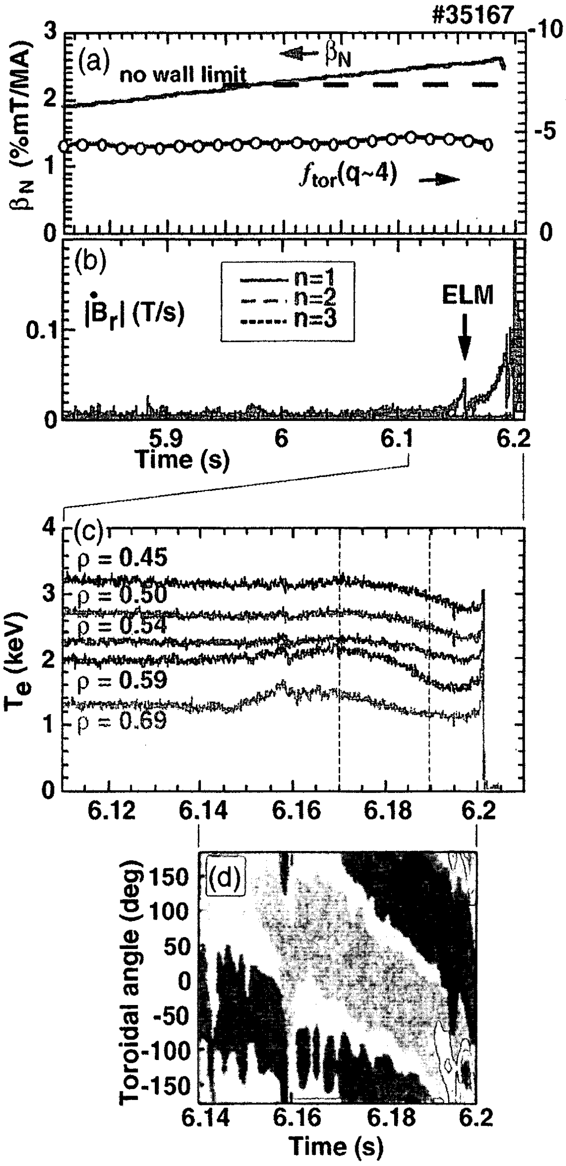

Fig. 7 Time history of a discharge (#35167) showing (a) β_N relative to the computed no-wall stability limit $\beta_N^{\text{no-wall}}$ and the plasma toroidal rotation frequency f_{tor} near the $q = 4$ surface, (b) $n = 1$, 2 and 3 components of time derivative of the perturbed magnetic field, (c) electron temperature T_e, and (d) a contour plot of time derivative of the perturbed radial magnetic field measured by saddle sensors at the occurrence of the $n = 1$ mode. The broken lines in Fig. 7(c) indicate the period for calculation of δT_e in Fig. 8.

resolution of the plasma rotation measurement by means of the CXRS is 16.7 ms [21]. No significant slowing down is observed on f_{tor} near the outer $q = 4$ surfaces before the growth of the $n = 1$ mode. Change in f_{tor} during the growth of the $n = 1$ mode is not measured within the time resolution. An eight saddle sensor array detected a growth of magnetic perturbations with $n = 1$ just before the disruption with $\gamma \approx 120\ \mathrm{s}^{-1}$ which is close to $\tau_w^{-1} \approx 100\ \mathrm{s}^{-1}$. Any other mode numbers such as $n = 2$ and $n = 3$ were not observed at the same time (Fig. 7(b)).

The time evolution of T_e suggests that the $n = 1$ mode with $\gamma \approx 120\ \mathrm{s}^{-1}$ is rotating at a period of ≈ 50 ms which corresponds to the toroidal rotation frequency of the $n = 1$ mode $f_{n=1} \approx 20$ Hz (Fig. 7(c)). A contour plot of the perturbed radial magnetic field clearly shows that the $n = 1$ mode with the growth rate of $\approx \tau_w^{-1}$ is rotating in the counter-direction to the plasma current (the same direction with the plasma rotation in the peripheral region) with the frequency $f_{n=1} \approx 20\ \mathrm{Hz} \approx 1/(2\pi\tau_w)$ (Fig. 7(d)).

A radial distribution of plasma radial displacement ξ_r due to the $n = 1$ mode estimated as $\xi_r = \delta T_e/\nabla T_e$ is shown in Fig. 8. Here the period for calculation of δT_e is indicated as broken lines in Fig. 7(c). A radial profile of theoretical plasma displacement of the unstable ideal $n = 1$ mode computed by the ERATO-J code is shown as a solid line in Fig. 8. The comparison of the experimental profile of ξ_r with the computed one is not straightforward in this case unlike the case of the RWM associated with current-driven kinks at low q^* since many significant poloidal modes exist in such a high q^* discharge. The experimental ξ_r profile is, however, similar to the theoretical one. Moreover, no evidence of

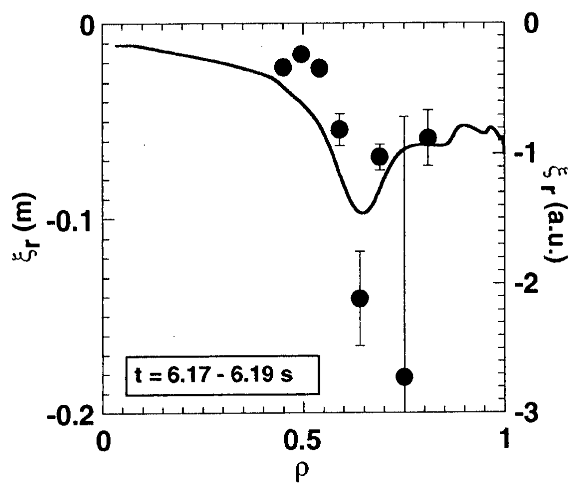

Fig. 8 A radial profile of radial plasma displacement due to the $n = 1$ mode estimated from T_e perturbations as $\xi_r = \delta T_e/\nabla T_e$ (closed circles), and a theoretical radial profile of the $n = 1$ radial plasma displacement computed by the ERATO-J code (a solid line). The error bars are mainly owing to uncertainty of ∇T_e.

magnetic islands nor a localized perturbation is observed at the same time.

Then, the MHD characteristics of the $n = 1$ mode emerged at $\beta_N \geq \beta_N^{\text{no-wall}}$ are in agreement with those of the RWM at high β predicted theoretically [8]. Thus, we concluded that the $n = 1$ mode is the RWM associated with the pressure-driven ideal $n = 1$ kink mode.

One of the differences of the pressure-driven RWMs at high β in JT-60U from those reported in DIII-D is that no clear reduction of the plasma toroidal rotation velocity is observed near the mode rational surfaces ($q = 4$) in JT-60U, while the rotation velocity in DIII-D continuously slows down before occurrence of the RWM until it is essentially zero just after the RWM onset [14,15]. Although f_{tor} does not decrease under the condition that $\beta_N \geq \beta_N^{\text{no-wall}}$, RWMs grow and are followed by major collapse or disruption in JT-60U. The result suggests that the toroidal rotation frequency $f_{tor} = 4$ kHz ($\approx 10^{-2} v_A/(2\pi R)$) is not sufficient for stabilization of the RWMs.

4. Collapses Following RWMs

Destabilization of the RWMs results in major collapse. In the case of the pressure-driven RWMs at high β, the RWMs is almost always followed by termination of the discharges, while discharges can be survived in the case of the current-driven RWMs at ~ zero β.

Small current quench occurs as a result of destabilization of the current-driven RWM at ~ zero β as shown in Fig. 1. The discharges are maintained after the current quench with the retained MHD activity. Termination of the discharge is often follows a few 100 ms after the small current quench caused by the MHD activity existing after the RWM and it is not clear whether the termination of discharge is directly led by the RWM or not. Detailed process of the collapse just after the RWM can bee seen through the time evolution of T_e and the perturbed magnetic field (Fig. 2). The $n = 1$ RWM grows with $\gamma \approx o(\tau_w^{-1})$ together with the change of T_e corresponding to the $n = 1$ radial plasma displacement. A thermal quench occurs only at the peripheral region after the RWM accompanied by higher n (= 2, 3) modes with a reduction of the $n = 1$ mode. The drop of the T_e by the thermal quench propagates into the core region within a few 10 ms with large $n = 1$ activity. Higher n modes appear occasionally corresponding to the thermal quenchs in the core region.

In contrast, a collapse due to destabilization of RWMs results in immediate termination of the discharge

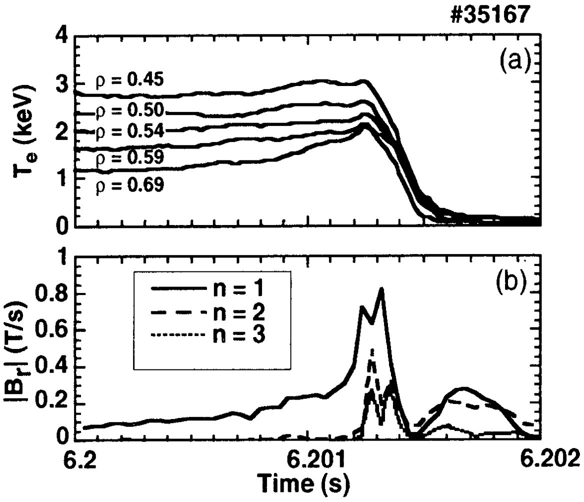

Fig. 9 Time evolution of (a) electron temperatures T_e and (b) n = 1, 2 and 3 components of time derivative of the perturbed magnetic field in the radial direction at the occurrence of the pressure-driven RWM at high β.

in the case of pressure-driven RWMs at high β. Figure 9 shows time evolution of T_e and n = 1, 2 and 3 components of time derivative of the perturbed magnetic field at a collapse caused by the pressure-driven RWM. The n = 1 RWM grows at $\gamma \approx$ 1,080 s^{-1} until $t \approx$ 6.2011 s and the growth rate of the n = 1 mode increases drastically to $\gamma > 10^4$ s^{-1}. A thermal quench occurs in the whole plasma region at $t \approx$ 6.2012 s accompanied by higher n ($n \geq 2$) magnetic perturbations. The time evolution of T_e suggests no significant change in the internal mode structure of the n = 1 mode at the drastic increase in the growth rate.

Comparing the process of collapses after the growth of the pressure-driven and current driven RWMs, it seems that excitation of higher n ($\geq$ 2) is important for thermal quenches in both cases and the drastic increase in the growth rate of the n = 1 mode larger than $10^2\ \tau_w^{-1}$ is a key phenomena for termination of discharges just after occurrence of the pressure-driven RWM.

5. Summary

Resistive wall modes are destabilized owing to the finite resistivity of the wall in the situation that ideal low n external kink modes are stable with a perfectly conducting wall but unstable without a wall. Ideal low n external kink modes are unstable in high β plasmas exceeding the $\beta_N^{\text{no-wall}}$ due to the effect of the plasma pressure. In such a case, RWMs which are associated with pressure-driven kink modes appear as a limiting instability of the attainable β. On the other hand, ideal low n external kink modes can be unstable even nearly at zero β due to the effect of the plasma current. In the latter case, RWMs associated with current-driven kink modes are observed. In this paper, RWMs associated with ideal current-driven and pressure-driven low n (n = 1) kink modes were investigated. Resistive wall modes associated with n = 1 current-driven external kink modes were identified through direct observation of the radial mode structure ξ_r. The current-driven RWMs destabilized at ~ zero β (β_N < 0.2) with fast current ramp-up ($\dot{I}_p$ = 0.5–1.2 MA/s) have the growth rate γ of 4–10 times τ_w^{-1}. No evidence of magnetic islands nor localized MHD activity which is typical for resistive instabilities is observed, while the time scale $\gamma \approx$ 4–10 τ_w^{-1} is in the range of resistive instabilities. Effects of the diamagnetic drift, which is a dominant fluid drift in such ohmic discharges, on the growth rate of the RWMs is not clear.

Resistive wall modes associated with pressure-driven n = 1 kink modes were also identified through direct observation of the radial mode structure ξ_r and other MHD characteristics such as the growth rate and the toroidal rotation frequency. No evidence of magnetic islands nor localized MHD activity is observed neither. The pressure-driven RWMs are observed in reversed shear discharges without a current ramp ($\dot{I}_p$ = 0) at high β (β_N > 2.4) in the range γ = 1–10 τ_w^{-1} with mode frequencies from nearly stationary to a few times $(2\pi\tau_w)^{-1}$. The pressure-driven RWMs occur with the plasma toroidal rotation of about 1% the Alfvén speed and no clear continuous slowing down of the plasma toroidal rotation is observed before the growth of the RWMs.

Occurrence of the n = 1 RWMs results in major collapse. In the case of current-driven RWMs at ~ zero β, the growth of the RWMs is followed by a thermal quench only at the peripheral region, then the drop of T_e propagates into the core region with the time scale of a few 10 ms. In the case of pressure-driven RWMs at high β, the growth of the RWMs is followed by a thermal quench in the whole plasma region and results in termination of the discharge just after the increase in the growth rate from $o(\tau_w^{-1})$ to larger than $10^2\ \tau_w^{-1}$. Why the growth rate of the n = 1 RWM mode can increase significantly with the similar internal mode structure is in analysis.

Concerning to pressure-driven RWMs, the experiments were carried out using the reversed shear discharge since the stability limit $\beta_N^{\text{no-wall}}$ is expected to be lower than those of normal shear discharges. It is, however, theoretically predicted that the MHD characteristics of RWMs depends on the current profile [13]. A study on current profile dependence of RWMs is also a future work although achievement of high β_N exceeding $\beta_N^{\text{no-wall}}$ with the limited heating power is a technical matter of RWM experiments.

Acknowledgements

The authors are grateful to Dr. M. Okabayashi and Dr. J. Manickam for fruitful discussions in collaboration between JAERI and the Princeton Plasma Physics Laboratory. The authors are also grateful to Prof. M. Wakatani, Prof. Z. Yoshida and Dr. T. Tatsuno for their theoretical suggestions.

References

[1] T. Ozeki *et al.*, *Plasma Physics and Controlled Nuclear Fusion Research*, Würzburg, 1992 (IAEA, Vienna, 1993) Vol.2, p.187.
[2] C. Kessel *et al.*, Phys. Rev. Lett. **72**, 1212 (1994).
[3] A.D. Turnbull *et al.*, Phys. Rev. Lett. **74**, 718 (1995).
[4] E.D. Fredrickson *et al.*, Phys. Plasmas **4**, 1589 (1997).
[5] E.J. Strait *et al.*, Phys. Plasmas **4**, 1783 (1997).
[6] Y. Ishii *et al.*, Plasma Phys. Control. Fusion **40**, 1607 (1998).
[7] S. Takeji *et al.*, J. Plasma Fusion Res. **76**, 575 (2000).
[8] A. Bondeson and D.J. Ward, Phys. Rev. Lett. **72**, 2709 (1984).
[9] J. Manickam *et al.*, Phys. Plasma **1**, 1601 (1994).
[10] Z. Yoshida and N. Inoue, Plasma Phys. Control. Fusion **27**, 245 (1985).
[11] M.S. Chu *et al.*, Phys. Plasmas **2**, 2236 (1995).
[12] J.M. Finn, Phys. Plasmas **2**, 198 (1995).
[13] A. Yoshioka *et al.*, J. Phys. Soc. Japan **67**, 3794 (1998).
[14] E.J. Strait *et al.*, Phys. Rev. Lett. **74**, 2483 (1995).
[15] A.M. Garofalo *et al.*, Phys. Rev. Lett. **82**, 3811 (1999).
[16] M. Okabayashi *et al.*, Nucl. Fusion **36**, 1167 (1996).
[17] C. Cates *et al.*, Phys. Plasmas **7**, 3133 (2000).
[18] E.J. Strait *et al.*, Nucl. Fusion **39**, 1977 (1999).
[19] A.M. Garofalo *et al.*, Nucl. Fusion **40**, 1491 (2000).
[20] S. Takeji *et al.*, Nucl. Fusion **42**, 5 (2002).
[21] Y. Koide *et al.*, Plasma Phys. Control. Fusion **36**, A195 (1994).
[22] N. Isei, M. Satoh, S. Ishida *et al.*, Rev. Sci. Instrum. **66**, 413 (1995).
[23] T. Tsunematsu *et al.*, Compt. Phys. Commun. **19**, 179 (1980).
[24] H. Yoshida *et al.*, Rev. Sci. Instrum. **66**, 143 (1995).
[25] T. Hatae *et al.*, Rev. Sci. Instrum. **70**, 772 (1999).
[26] T. Fukuda *et al.*, Rev. Sci. Instrum. **60**, 1080 (1989).
[27] Y. Kawano *et al.*, Rev. Sci. Instrum. **67**, 1520 (1996).
[28] T. Fujita *et al.*, Fusion Eng. Des. **34&35**, 289 (1997).
[29] K. Tani *et al.*, Phys. Soc. Jpn. **50**, 1726 (1981).
[30] Y. Koide *et al.*, in *Plasma Physics and Controlled Nuclear Fusion Research*, Würzburg, 1992 (IAEA, Vienna, 1993) Vol.1, p777.